APPLIED GEOPHYSICS, Vol.14, No.2 (June 2017), P. 247–257, 4 Figures.
DOI: 10.1007/s11770-017-0617-x

Research and application of spectral inversion technique in frequency domain to improve resolution of converted PS-wave*

Zhang Hua♦[1,2,3,4], He Zhen-Hua[1,2], Li Ya-Lin[3,4], Li Rui[1,2], He Guamg-Ming[3,4], and Li Zhong[3,4]

Abstract: Multi-wave exploration is an effective means for improving precision in the exploration and development of complex oil and gas reservoirs that are dense and have low permeability. However, converted wave data is characterized by a low signal-to-noise ratio and low resolution, because the conventional deconvolution technology is easily affected by the frequency range limits, and there is limited scope for improving its resolution. The spectral inversion techniques is used to identify λ/8 thin layers and its breakthrough regarding band range limits has greatly improved the seismic resolution. The difficulty associated with this technology is how to use the stable inversion algorithm to obtain a high-precision reflection coefficient, and then to use this reflection coefficient to reconstruct broadband data for processing. In this paper, we focus on how to improve the vertical resolution of the converted PS-wave for multi-wave data processing. Based on previous research, we propose a least squares inversion algorithm with a total variation constraint, in which we uses the total variance as a priori information to solve under-determined problems, thereby improving the accuracy and stability of the inversion. Here, we simulate the Gaussian fitting amplitude spectrum to obtain broadband wavelet data, which we then process to obtain a higher resolution converted wave. We successfully apply the proposed inversion technology in the processing of high-resolution data from the Penglai region to obtain higher resolution converted wave data, which we then verify in a theoretical test. Improving the resolution of converted PS-wave data will provide more accurate data for subsequent velocity inversion and the extraction of reservoir reflection information.
Keyword: spectral inversion, resolution, broadband wavelet, thin reservoir

Introduction

Multi-wave exploration is advantageous in reservoir and structural imaging, lithology and fluid identification, and crack detection. Converted PS-wave data is characterized by a low signal-to-noise (S/N) ratio and low resolution. The frequency range of a single shot is

Manuscript received by the Editor Februay 25, 2016; revised manuscript received April 26, 2017.
*This work was supported by the China National Petroleum Corporation Scientific research and technology development project (Nos. 2013E-38-08).
1.State Key Laboratory of Oil and Gas Reservoir Geology and Exploitation, Chengdu 610059, China.
2. College of Geophysics,Chengdu University of Technology, Chengdu 610059, China.
3. Geophysical Exploration Company, Chuanqing Drilling Engineering Co.Ltd., CNPC, Chengdu 610213, China.
4. Mountain Geophysical Technology Test Center, CNPC, Chengdu 610213, China
♦Corresponding author: Zhang Hua (Email: zhanghua_sc@cnpc.com.cn)

narrow, the effective reflection energy is weak, and its continuity is poor, so it is difficult to extract reservoir reflection information. To improve the resolution of the converted PS-wave target layer, the frequency band must be broadened.

After conventional deconvolution processing, the resolution of shallow layer data can be improved, but the ability to improve the resolution of the deep target layer is limited and the thin-layer recognition ability is weak. Partyka et al. (1999) found that discrete Fourier spectral decomposition can be used to increase the resolution of seismic data. Portniaguine (2004) proposed the spectral inversion method, which can obtain the reflection coefficient while also improving the layer thickness. Puryear and Castagna (2008) proposed a multi-layer geological objective function for the spectral inversion method and obtained reasonable information regarding the formation thickness by solving the objective function. Chopra et al. (2009) used the spectral inversion techniques to invert the reflection coefficients of thin-layer data, and was able to detect thin subtle anomalies from the inversion results. Yuan et al. (2009) proposed a global optimization algorithm known as the particle swarm optimization inversion algorithm that attempts to improve the accuracy and stability of spectral inversion. Nguyen and Castagna (2010) used logging information to successfully control the spectral inversion of the reflection coefficient, which can improve its inversion fidelity. Yang et al. (2011) used the matching tracking algorithm to conduct spectral inversion of the reflection coefficient and obtained a good resolution of the thin layer. To improve the accuracy of the inversion algorithm, Zhang and Castagna (2011) used a model as a priori information to conduct spectral inversion. Chai et al. (2012) used the LSQR algorithm to evaluate the spectral inversion model and found that a better inversion algorithm could improve the accuracy of the reflection coefficient. Oyem et al. (2013) conducted a detailed analysis of spectral inversion in the time-frequency domain to improve the resolution of the thin-layer thickness, which yields a significant advantage in breaking up the bottleneck associated with conventional deconvolution techniques. Yuan et al. (2013) investigated the sparse Bayesian inversion method in the frequency domain and used the spectral inversion method to identify the thin layer, thereby recovering more information from outside the frequency band of the seismic data. Zhou et al. (2014) used the spectral inversion method to improve the resolution of thin reservoirs and successfully identified both oil and water reservoirs. Using the reflection coefficient and broadband wavelet, Chi et al. (2015) reconstructed thin sand body data, which can distinguish the Fuyu oil layer, and successfully predicted the compact sand body. Liu et al. (2016) used the basis pursuit spectral inversion algorithm to improve the resolution of deep reservoirs and the accuracy of reservoir fluid identification. In short, the continuous application of spectral inversion technology worldwide has proved its merits with respect to improving thin-layer resolution and identified the need for a stable inversion algorithm to improve inversion accuracy for a wideband wavelet extraction technology.

In view of the low resolution of converted PS-wave data, we must broaden its spectrum and improve its vertical resolution to increase it similarity with the PP-wave. Based on previous research, in this paper, we use total variance as a priori information to help solve under-determined problems. We propose a least squares inversion algorithm based on the total variation constraint to improve the accuracy and stability of the inversion and use the Gaussian fitting amplitude spectrum to simulate wide-band wavelet data. We then apply this technology in the Penglai region for high-resolution data recovery processing and obtain a higher resolution converted wave, which will facilitate subsequent multi-wave inversion and reservoir prediction.

Methods and principles

Spectral inversion algorithm with total variance constraints in frequency domain

According to the theory of seismic signal processing and analysis, using the spectral information in seismic wavelet and seismic data, we can construct an inversion objective function using the reflection coefficient, which is composed of parity components in the frequency domain. We can express the multi-layer model objective function in the frequency domain as shown in equation (1) (Puryear and Castagna, 2008):

$$\begin{aligned} &\mathrm{O}(\mathbf{r}_e,\mathbf{r}_o,T,t) \\ &= \int_{f_{Low}}^{f_{High}} \left[a_e \left\{ \begin{array}{l} \mathrm{Re}\left[\dfrac{\mathbf{S}(t,f)}{\mathbf{W}(t,f)} e^{-i2\pi f\Delta t} \right] \\ -\int_{-t_w}^{t_w} \mathbf{r}_e(t)\cos(\pi f T(t))dt \end{array} \right\} \right. \\ &\left. + a_o \left\{ \begin{array}{l} \mathrm{Im}\left[\dfrac{\mathbf{S}(t,f)}{\mathbf{W}(t,f)} e^{-i2\pi f\Delta t} \right] \\ -\int_{-t_w}^{t_w} \mathbf{r}_o(t)\sin(\pi f T(t))dt \end{array} \right\} \right] df. \end{aligned} \tag{1}$$

In equation (1), $\mathbf{S}(t, f)$ is the amplitude spectrum of the seismic data, $\mathbf{W}(t, f)$ is the amplitude spectrum of the wavelet, $a_o(t)$ and $a_e(t)$ are the odd–even weight coefficients, respectively, $r_o(t)$ and $r_e(t)$ are the odd–even components of the reflection coefficient, respectively, T is the time thickness, and t_w is the half-window length.

To facilitate computation, we write equation (1) as a discrete odd–even matrix, as follows:

$$\begin{bmatrix} \mathrm{Re}\left(\frac{S(f_1)}{W(f_1)} * e^{i2\pi f_1 \Delta t}\right) \\ \mathrm{Re}\left(\frac{S(f_2)}{W(f_2)} * e^{i2\pi f_2 \Delta t}\right) \\ \vdots \\ \mathrm{Re}\left(\frac{S(f_m)}{W(f_m)} * e^{i2\pi f_m \Delta t}\right) \end{bmatrix} = \begin{bmatrix} cos(\pi T_1 f_1) & cos(\pi T_2 f_1) & \cdots & cos(\pi T_{N/2} f_1) \\ cos(\pi T_1 f_2) & cos(\pi T_2 f_2) & \cdots & cos(\pi T_{N/2} f_1) \\ \vdots & \vdots & \vdots & \vdots \\ cos(\pi T_1 f_M) & cos(\pi T_2 f_M) & \cdots & cos(\pi T_{N/2} f_M) \end{bmatrix} \cdot \begin{bmatrix} 2r_e(t_1) \\ 2r_e(t_2) \\ \vdots \\ 2r_e(t_{N/2}) \end{bmatrix},$$

$$\begin{bmatrix} \mathrm{Im}\left(\frac{S(f_1)}{W(f_1)} * e^{i2\pi f_1 \Delta t}\right) \\ \mathrm{Im}\left(\frac{S(f_2)}{W(f_2)} * e^{i2\pi f_2 \Delta t}\right) \\ \vdots \\ \mathrm{Im}\left(\frac{S(f_m)}{W(f_m)} * e^{i2\pi f_m \Delta t}\right) \end{bmatrix} = \begin{bmatrix} sin(\pi T_1 f_1) & sin(\pi T_2 f_1) & \cdots & sin(\pi T_{N/2} f_1) \\ sin(\pi T_1 f_2) & sin(\pi T_2 f_2) & \cdots & sin(\pi T_{N/2} f_1) \\ \vdots & \vdots & \vdots & \vdots \\ sin(\pi T_1 f_M) & sin(\pi T_2 f_M) & \cdots & sin(\pi T_{N/2} f_M) \end{bmatrix} \cdot \begin{bmatrix} 2r_o(t_1) \\ 2r_o(t_2) \\ \vdots \\ 2r_o(t_{N/2}) \end{bmatrix}. \quad (2)$$

Then, we can abbreviate equation (2), as follows:

$$\begin{aligned} \mathbf{b}_e &= \mathbf{A}_e \times \mathbf{R}_e, \\ \mathbf{b}_o &= \mathbf{A}_o \times \mathbf{R}_o, \end{aligned} \quad (3)$$

where $\mathbf{b}_o(t)$ and $\mathbf{b}_e(t)$ are parity components of the wavelet correlation matrix, $\mathbf{A}_o(t)$ and $\mathbf{A}_e(t)$ are parity components of the weight matrix, and $\mathbf{R}_o(t)$ and $\mathbf{R}_e(t)$ are parity components of the reflection coefficient matrix.

In accordance with equations (1)–(3), we can express the objective function as follows:

$$\mathrm{O}(r_e, r_o) = \left\| \begin{bmatrix} a_e(\mathbf{b}_e - \mathbf{A}_e \times \mathbf{R}_e) \\ a_o(\mathbf{b}_o - \mathbf{A}_o \times \mathbf{R}_o) \end{bmatrix} \right\|_2^2. \quad (4)$$

There are many algorithms for solving the objective function (equation (4)). Here, we use total variance as a priori information, propose a least squares inversion algorithm based on the total variation constraint to improve its stability, and obtain the optimal solution with a highly accurate objective function.

If we write this objective function (equation (4)) as a more general optimization problem, we obtain the objective function expressed in equation (5):

$$\mathbf{b} = \mathbf{A}\mathbf{x}, \quad (5)$$

where $\mathbf{x}$ is the desired reflection coefficient matrix.

In equation (5), we can express the objective function of the weighted least squares estimation as follows:

$$\min_{\mathrm{x}} \mathrm{f(x)} = \frac{1}{2}(\mathbf{A}\mathbf{x} - \mathbf{b})^T \mathbf{W}^{-1}(\mathbf{A}\mathbf{x} - \mathbf{b}), \quad (6)$$

where $\mathbf{W}$ is the diagonal weight matrix.

If we add a total variation item to the objective function in equation (6), we obtain:

$$\mathrm{TV}(x) = \sum_{i,j \in \mathbf{Q}} \sqrt{(x_{i,j} - x_{i-1,j})^2 + (x_{i,j} - x_{i,j-1})^2}, \quad (7)$$

where $\mathbf{D}$ is the set of profiles and $x_{i,j}$ is the jth element of the i-th row.

We can convert the objective function problem in equation (6) into the objective function in equation (8), as follows:

$$\arg\min_{x} \frac{1}{2}(\mathbf{A}\mathbf{x} - \mathbf{b})^T \mathbf{W}^{-1}(\mathbf{A}\mathbf{x} - \mathbf{b}) + \beta\, \mathrm{TV}(x), \quad (8)$$

where β is a weight coefficient greater than zero.

If we then introduce the intermediate variable z, according to Lagrange's theorem, we can convert

the solution of equation (8) into an unconstrained optimization problem (equation (9)):

$$\arg\min_x \frac{1}{2}(\mathbf{Ax}-\mathbf{b})^T\mathbf{W}^{-1}(\mathbf{Ax}-\mathbf{b}) + \beta\,\mathrm{TV}(z)+\frac{1}{2}\alpha\left\|x-z\right\|_2^2, \quad (9)$$

where α is the Lagrange penalty factor.

The necessary condition for the optimal solution of equation (9) is $\left\|x-z\right\|_2^2=0$, so the optimal solution of equation (9) is also the solution for equation (8). Then, the optimization problem of equation (9) can use the relaxation method of alternating iterations. We can decompose the solution of equation (9) into two equations:

$$x^k=\arg\min_x \frac{1}{2}\left\|\mathbf{A}x^k-\mathbf{b}\right\|_2^2+\frac{1}{2}\alpha\left\|x^k-z^k\right\|_2^2, \quad (10)$$

$$z^k=\arg\min_x \beta\,\mathrm{TV}(z^k)+\frac{1}{2}\alpha\left\|x^{k+1}-z^k\right\|_2^2. \quad (11)$$

Since the objective function of equation (10) is a quadratic convex optimization problem, an optimal solution exists. So, we can obtain the linear equation for equation (10). We can iteratively obtain the solution for x using the following relaxation iteration equation:

$$x^{k+1}=x^k+\lambda\mathbf{D}^{-1}\left[\mathbf{A}^T\mathbf{W}^{-1}\mathbf{b}+\alpha z-(\mathbf{A}^T\mathbf{W}^{-1}\mathbf{A}+\alpha\mathbf{I})x^k\right], \quad (12)$$

where **D** is a diagonal matrix, in which the main diagonal elements consist of $\mathbf{A}^T\mathbf{W}^{-1}\mathbf{b}+a\mathbf{I}$, and the relaxation factor is in the range $0<1<2$.

After solving the optimal solution x^{k+1} of equation (10), we can solve for the total variation minimization using equation (11). We can then directly derive the objective function and obtain the optimal iteration equation, as follows:

$$z^{k+1}=x^{k+1}-\frac{\beta}{\alpha}\frac{\partial\,\mathrm{TV}(z^k)}{\partial z^k}. \quad (13)$$

We obtain the optimal solution for the objective function by equations (12) and (13) as the initial solution of the next iteration until the iterative condition is satisfied, thereby finding the optimal solution for the objective function.

High-resolution data recovery using wideband wavelet

After obtaining the high-precision reflection coefficient by spectral inversion, we must perform high-resolution data recovery. Generally, we achieve high-frequency reconstruction with the high-frequency wavelet or Yu-shi wavelet (Yu, 1996; Cai, 2000). However, although this method can obtain high-resolution processing data, the low-frequency aspect of the seismic data will inevitably be missing.

Many geophysicists believe the low-frequency component of reflected wave data and anomalous records, such as underground rock pores and fluids, are a rich source of information, so the potential significance and technical application value of retaining low-frequency data are paid increasing attention by data interpreters.

Here, we extract the wide-frequency wavelet by the Gaussian fitting method to maintain the low frequencies and extend the high frequencies, and then perform high-resolution recovery processing with this wavelet to obtain a high-resolution converted PS-wave profile with low-frequency information.

We assume that the Gaussian fitting amplitude spectrum function $\mathrm{f}(\omega)$ of the converted PS-wave before high-resolution processing is as follows:

$$\mathrm{f}(\omega)=K\exp\left[-\frac{(\omega-\omega_0)^2}{L^2}\right], \quad (14)$$

where ω is frequency and K and L are pending frequency parameters.

From both sides of equation (14), we take the logarithm and shift items as follows:

$$-\ln\left[\mathrm{f}(\omega)\right]=\frac{\omega^2}{L^2}-\frac{2\omega\omega_0}{L^2}+\frac{\omega_0^2}{L^2}-\ln K. \quad (15)$$

Let $s=-\ln\left[\mathrm{f}(\omega)\right]$, $a=\frac{1}{L^2}$, $b=-\frac{2\omega_0}{L^2}$, $c=\frac{\omega_0^2}{L^2}-\ln K$ in equation (15), then we can reduce equation (15) to equation (16):

$$\mathbf{s}=a\boldsymbol{\omega}^2+b\boldsymbol{\omega}+c. \quad (16)$$

Then, the error squared sum between logarithm **s** of the Gaussian fitting spectrum and logarithm $\bar{\mathbf{s}}$ of the discrete amplitude spectrum of the converted wave is as follows:

$$E=\sum_i^n(\mathbf{s}_i-\bar{\mathbf{s}}_i)^2. \quad (17)$$

If we then bring equation (16) into equation (17) and the derivative of the pending parameter is zero, the values of parameters a, b, c are as follows:

$$\begin{bmatrix} a \\ b \\ c \end{bmatrix} = \begin{bmatrix} \sum_i \omega_i^4 & \sum_i \omega_i^3 & \sum_i \omega_i^2 \\ \sum_i \omega_i^3 & \sum_i \omega_i^2 & \sum_i \omega_i \\ \sum_i \omega_i^2 & \sum_i \omega_i & n \end{bmatrix}^{-1} \times \begin{bmatrix} \sum_i \omega_i^2 \bar{s}_i \\ \sum_i \omega_i \bar{s}_i \\ \sum_i \bar{s}_i \end{bmatrix}. \quad (18)$$

By solving equation (18), we can obtain the pending parameter value of the curve fitting spectrum in equation (14):

$$\begin{cases} K = \exp(\frac{b^2}{4a} - c) \\ L = \frac{1}{\sqrt{a}} \\ \omega_0 = -\frac{b}{2a} \end{cases}. \quad (19)$$

We can plot the converted PS-wave Gaussian fitting amplitude spectrum in equation (14) on the interactive panel and use the Gaussian fitting curve to extend the high-frequency amplitude spectrum into the broadband amplitude spectrum, while maintaining the low-frequency amplitude information. We can then use this broadband amplitude spectrum as the amplitude spectrum of the Ricker wavelet or Yu wavelet, obtain the broadband wavelet in the time domain, and reconstruct the high-resolution converted PS-wave data using the reflection coefficient convolution and the broadband wavelet.

Model building and field data application

Thin lens interbedding model for spectral inversion

First, we established a thin lens body interbedding velocity model with small velocity changes. The velocity of each layer is shown in Figure 1a, the velocity model grid contains 1000 × 2000 points, and the overall grid size is 20 m × 10 m. We used this model to conduct a forward simulation with a 30-Hz Ricker wavelet, with a spatial sampling interval of 20 m and a time sampling interval of 1 ms, and obtained the forward profile (Figure 1b), the resolution of which is obviously low.

We obtained the inversion results of Figures 1c and 1d by reflection coefficient inversion using the conjugate gradient inversion algorithm and the inversion algorithm proposed in this paper, respectively. From the analyses shown in Figures 1c and 1d, compared with the traditional conjugate gradient inversion technique, we see that the spectral inversion algorithm can obtain a reflection coefficient with high polarity, position accuracy, and S/N ratio.

To obtain high-frequency profiles, we performed convolution processing using the reflection coefficients of Figures 1c and 1d and the 50-Hz Ricker wavelet, respectively, as shown in Figures 1e and 1f. By comparing and analyzing Figures 1e and 1f, we found the resolution of the recovered high-frequency profile to be significantly higher than that of Figure 1b, thus proving that we can improve the profile resolution by using the spectral inversion method. At the same time, because the reflection coefficient accuracy and S/N ratio of Figure 1d is significantly higher than those of Figure 1c, the resolution and S/N ratio of the profile (Figure 1f) after convolution processing are also much better than those in Figure 1e. This proves that the high-precision reflection coefficient provides the basis for subsequent high-frequency profile recovery.

Resolving $\lambda/8$ thickness by spectral inversion using a wedge model

We established a wedge velocity model with low velocity (Figure 2a), in which the velocity of the wedge is 1300 m/s, the velocity of the other regions is 2100 m/s, the velocity model grid contains 140 × 1000 points, and the overall grid size is 10 m × 10 m. We used this model to conduct a forward simulation with the 35-Hz Ricker wavelet. Using a spatial sampling interval of 20 m and a time sampling interval of 1 ms, we obtained the forward profile (Figure 2b), from which we can distinguish only a 20-m wedge thickness.

To improve the resolution of the profile in Figure 2b, we used conventional predictive deconvolution with a prediction step length of 8 ms. As shown in Figure 2c, the resolution of this profile is improved to a certain extent in that we can distinguish a 12-m wedge thickness, but we still cannot obtain its tuning resolution thickness, and this method inevitably produces noise interference.

Next, we obtained the reflection coefficient and zero-

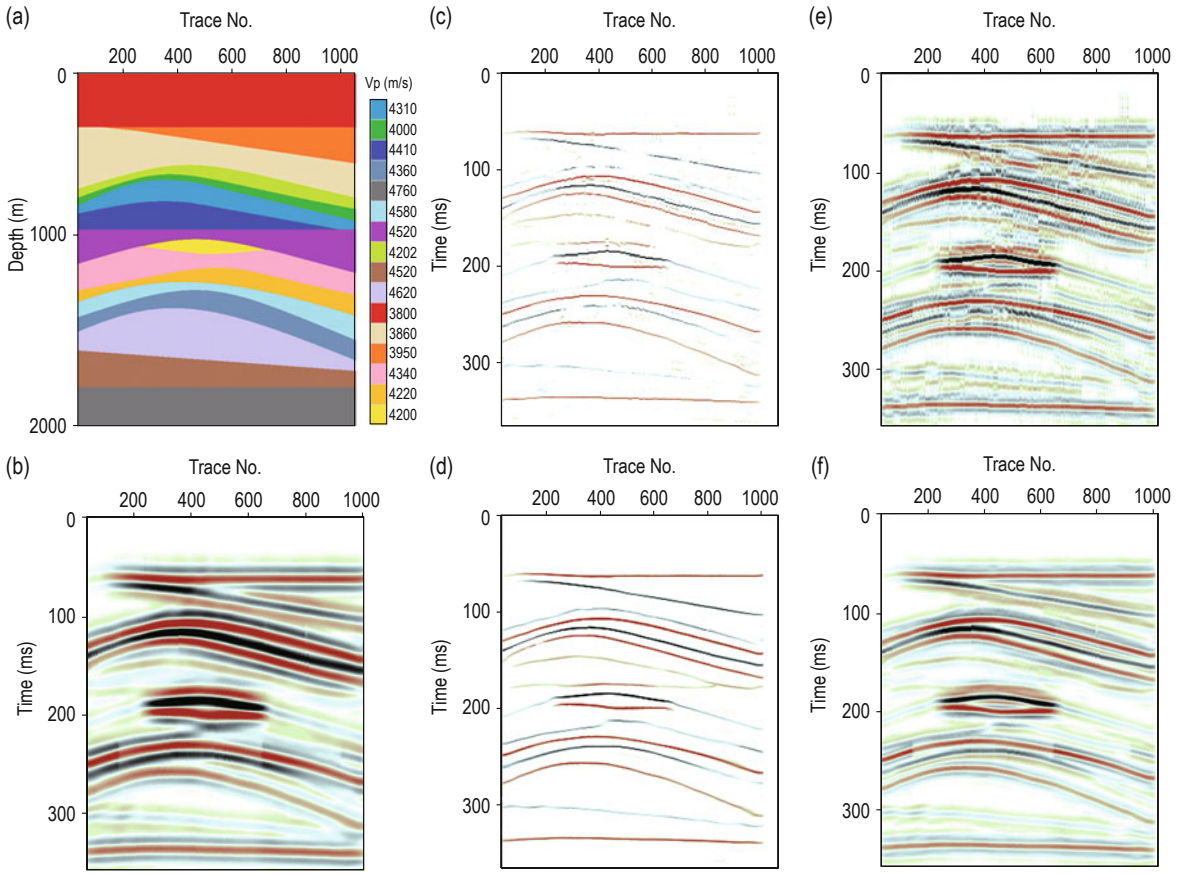

Fig.1 Thin lens interbedding model for spectral inversion experiment, (a) thin lens interbedding model, (b) 30-Hz forward data, (c) reflection coefficient obtained by traditional conjugate gradient spectral inversion algorithm, (d) reflection coefficient obtained by our proposed spectral inversion algorithm, (e) 50-Hz high-frequency recovery profile using the data in Figure 1c, (f) 50-Hz high-frequency recovery profile using the data in Figure 1d.

phase broadband wavelet using the method we propose in this paper. The obtained reflection coefficient (Figure 2d) is more accurate and has less noise interference. The main and side lobes of the broadband wavelet (Figure 2e) are also well compressed, and there is less side lobe interference. We then performed a high-resolution data recovery process using the broadband wavelet (Figure 2e) and the reflection coefficient (Figure 2d) to obtain a higher resolution record (Figure 2f). From the analyses shown in Figures 2d–2h, we can conclude the following: Using this method, the reconstructed high-resolution data (Figure 2f) can reach 4 m in thickness, which exceeds the thickness limit of $\lambda/8 = 4.64$ m. Because the broadband wavelet involved in the reconstruction maintains low-frequency information, this data not only effectively expands the high-frequency amplitude spectra, but also retains the low-frequency component (Figure 2h), which proves that this method can break up the bottleneck experienced in conventional frequency technology and distinguish the thin layer to the greatest extent.

High-resolution processing in the multi-wave data model

Based on the stratum structure of actual data in the Penglai area, we established the 5-layer velocity model shown in Figure 3a, in which the number of grid points is 200 × 2000; the overall grid size is 10 m × 10 m; the P-wave velocities are, respectively, $v1 = 1200$ m/s, $v2 = 2000$ m/s, $v3 = 2500$ m/s, $v4 = 2900$ m/s, and $v5 = 4000$ m/s; the V_p/V_s ratio is $\sqrt{3}/1$; the low-frequency Ricker wavelet is a P-wave source; the spatial sampling interval is 10 m; and the time sampling interval is 1 ms. We used the model to conduct a forward simulation using the time–distance curve equation for elastic wave field separation (Li, 2007). We obtained shots of the PP and PS reflected waves, and then obtained the post-migration stack profiles after the cut, gather sort, migration, and

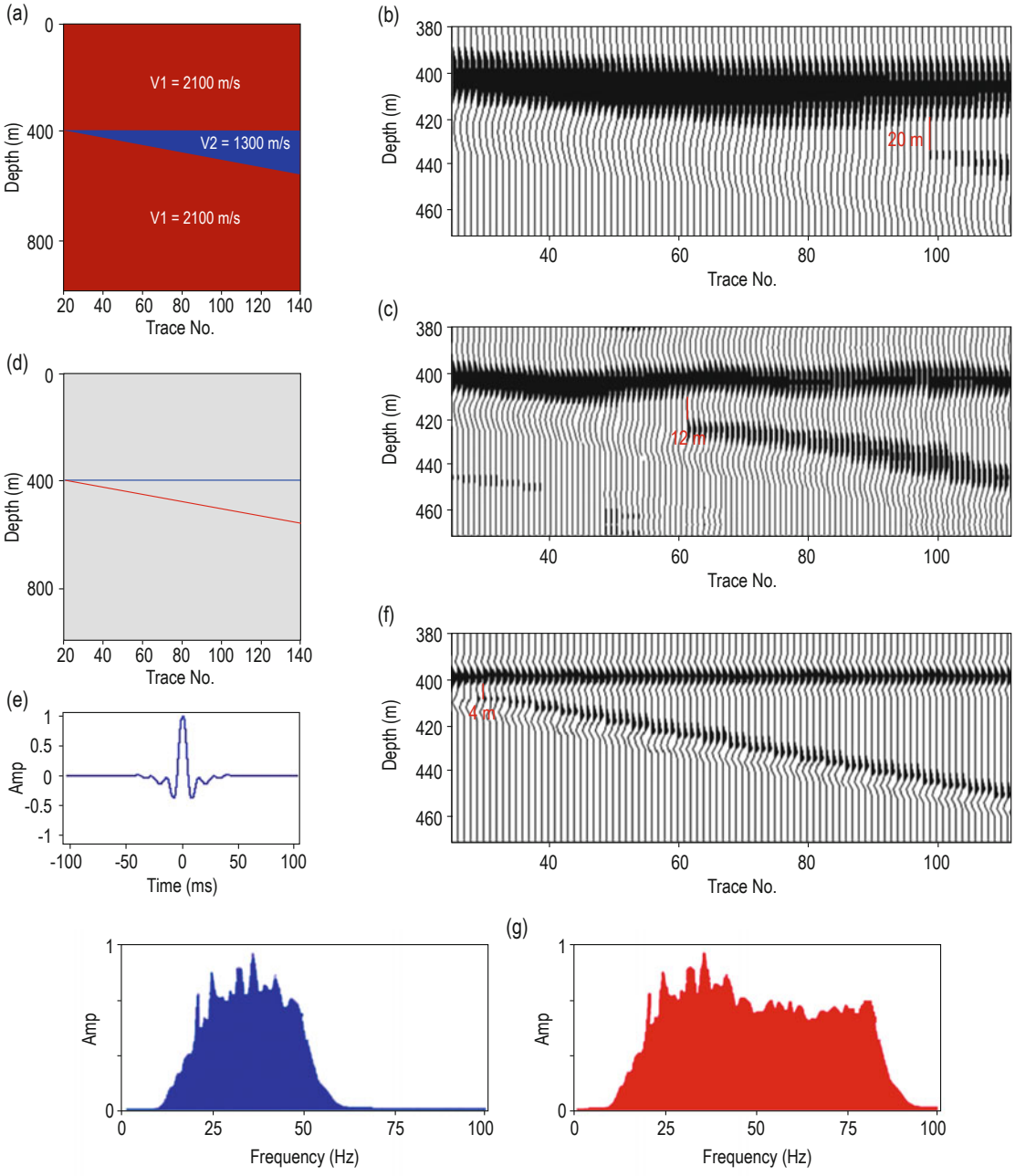

Fig.2 Experimental spectral inversion results for resolving $\lambda/8$ thickness using a wedge model. (a) wedge-shaped model with low velocity, (b) 35-Hz synthetic record, (c) results using conventional deconvolution method, (d) reflection coefficient obtained by the spectral inversion algorithm proposed in this paper, (e) broadband wavelet obtained by the Gaussian fitting method of this paper, (f) high-resolution data obtained by the method proposed in this paper, (g) amplitude of Fig. 2(b) and Fig. 2(f).

other shot preprocessing steps. Figure 3b shows the P-wave stack data with a 25-Hz main frequency after processing, and Figure 3c shows the converted PS-wave stack data with a 15-Hz main frequency after processing. We can see that the resolutions of the P-wave and the converted PS-wave profiles are all low and the horizon information cannot be effectively matched.

Then, we performed reflection coefficient spectral inversion processing on Figures 3b and 3c to obtain the reflection coefficient (Figure 3d) and the PS-wave reflection coefficient (Figure 3e) with higher resolutions than those of the original profile. We reconstructed the data using a 35-Hz broadband wavelet to obtain the high-resolution P-wave profile (Figure 3f) and the

converted PS-wave profile (Figure 3g). The results (Figures 3f−3g) show that the resolutions of the P-wave and converted PS-wave data are obviously improved, with richer layer information, and the identified horizon information is convenient for subsequent multi-wave horizon matching process, thereby proving that this method can achieve the desired effect in multi-wave high-resolution processing.

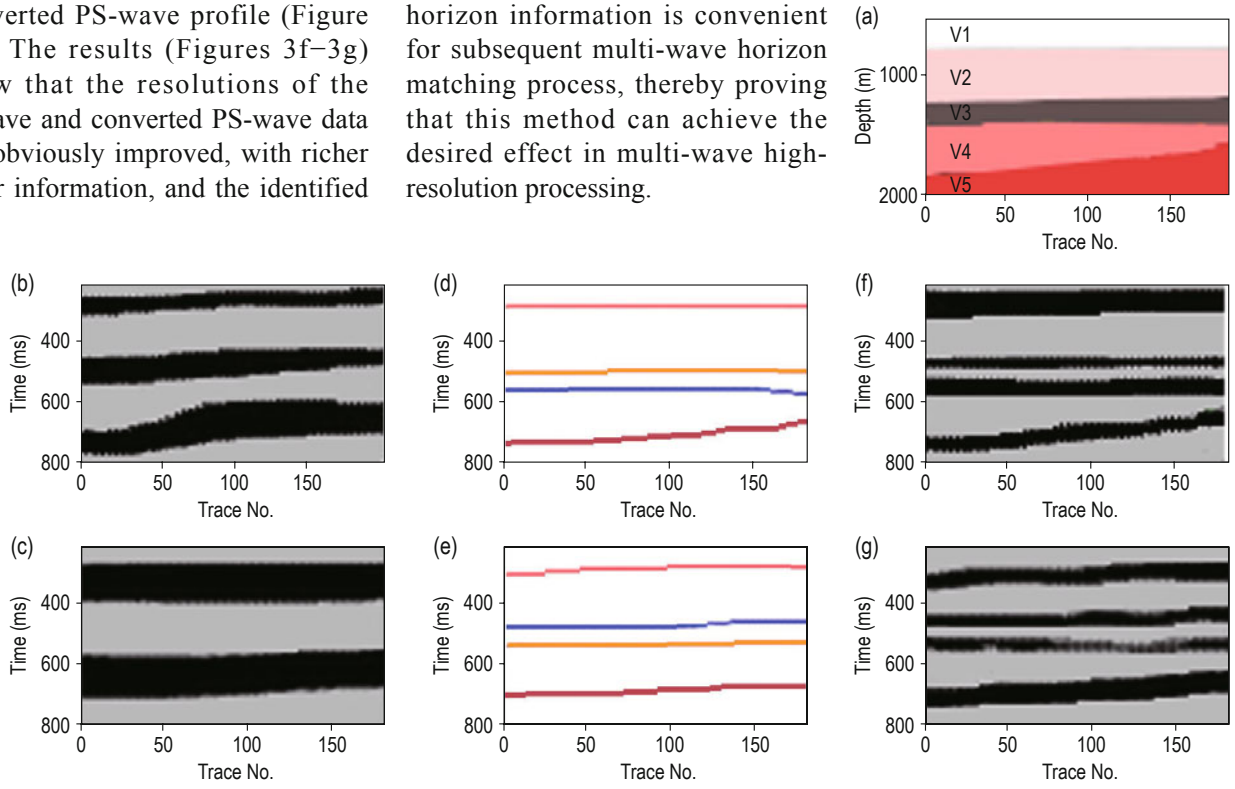

Fig.3 High-resolution processing results for the multi-wave data model: (a) velocity model, (b) forward profile of PP-wave, (c) forward profile of converted PS-wave, (d) PP-wave reflection coefficient obtained by spectral inversion, (e) converted PS-wave reflection coefficient obtained by spectral inversion, (f) broadband recovery data for a PP-wave, and (g) broadband recovery data for a converted PS-wave.

Application of real converted PS-wave data

To further determine the distribution of the Xujiahe Formation reservoirs in the study area, we used the difference between the PP-wave and the converted PS-wave, and performed a multi-wave exploration in the Penglai South area. This area is located in the middle trending tectonic belts in the middle of Sichuan Province. The sandstone and mudstone receiving conditions of the surface outlet are good, but the gravel in the outflow along the river is less favorable. Due to the large population density and wide span of the target layer, the S/N ratio of the seismic data recorded by the multi-component digital detector was low and the frequency range was narrow. Specifically, in processing the main frequency of the converted PS-wave, we found that it reached 20 Hz but not the 30 Hz of the PP-wave. Therefore, the resolution of the converted PS-wave must be improved while maintaining the S/N ratio, which has been an ongoing difficulty in converted PS-wave processing. To verify the practical application effect of our proposed theories and methods, we selected the target layer of the converted PS-wave in the Penglai area of the Sichuan Basin for application testing, as shown in Figure 4.

The results of our comparison of the high-resolution effects of converted PS-waves before and after processing (Figures 4a–4c) suggest that by using this method, the resolution is obviously improved, the construction details are obvious, the fault is clearer, the frequency is increased from 20 Hz to 30 Hz, and the frequency band is effectively expanded by retaining the low-frequency information.

Comparative analysis of the logging synthetic records (Figures 4d −4g): The converted PS-wave data before high-resolution processing matches only the 20-Hz logging record, the resolution of the velocity inversion is not high, and the low-velocity reservoir cannot be resolved. In contrast, the converted PS-wave data after high-resolution processing better matches the 30-Hz logging record, the resolution of the velocity inversion is obviously improved, and the low-veolocity and high-porosity sandstone reservoir segment is more easily identified, which lays a solid foundation for the quantitative prediction of subsequent reservoirs.

As the vibration characteristics

differ in the PP-wave and the converted PS-wave, the same tectonic wave will have different responses. As shown in Figures 4b and 4h, their fault recognition ability differs, which reveals the advantage of multi-wave joint interpretation.

As shown in Figure 4i, the gas well is located in the strong amplitude region (red-yellow) of the PP-wave and in the weak amplitude region (blue-green) of the PS-wave. This is consistent with the predicted results of the gas phase in the reservoir, in which the reflection of

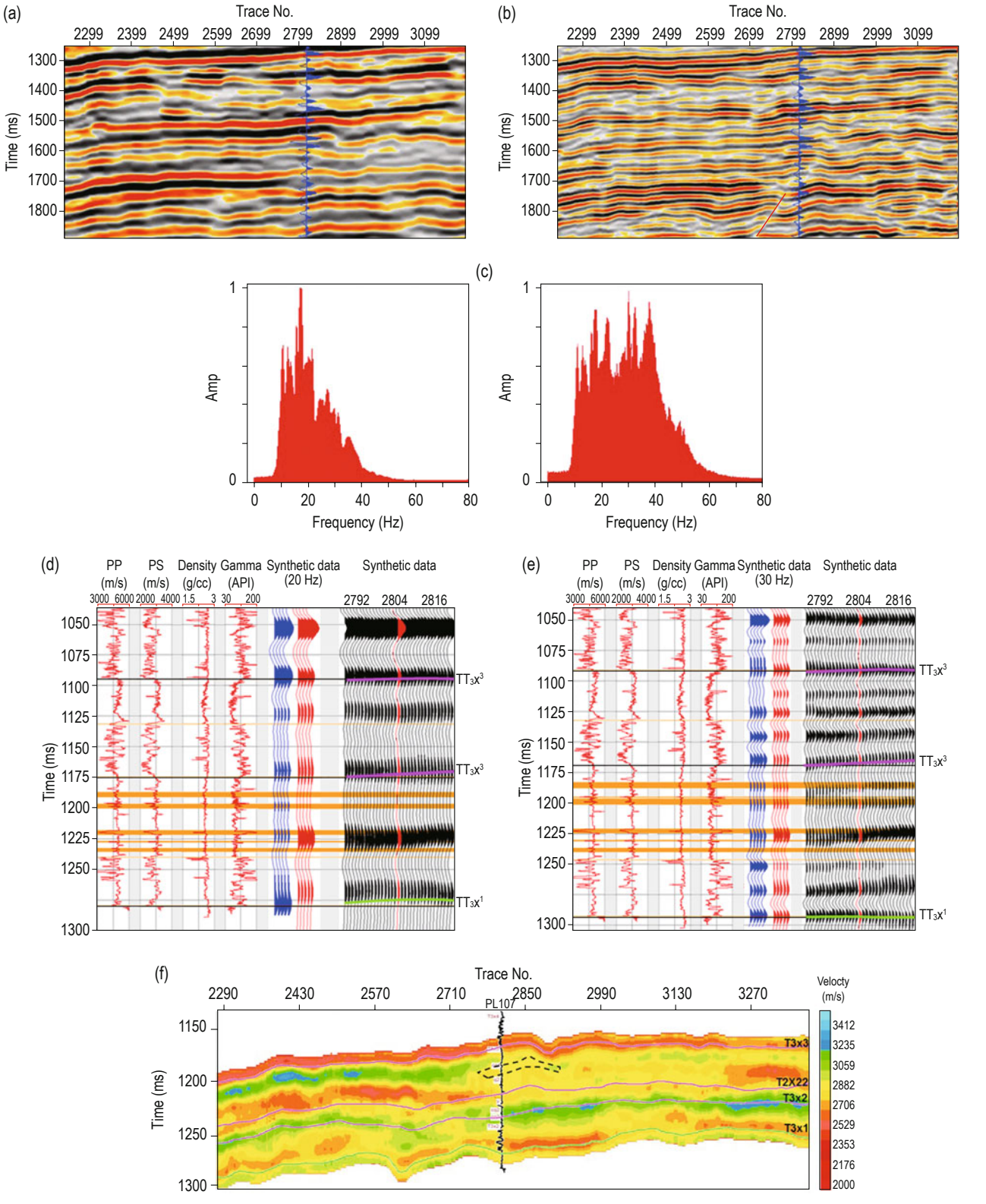

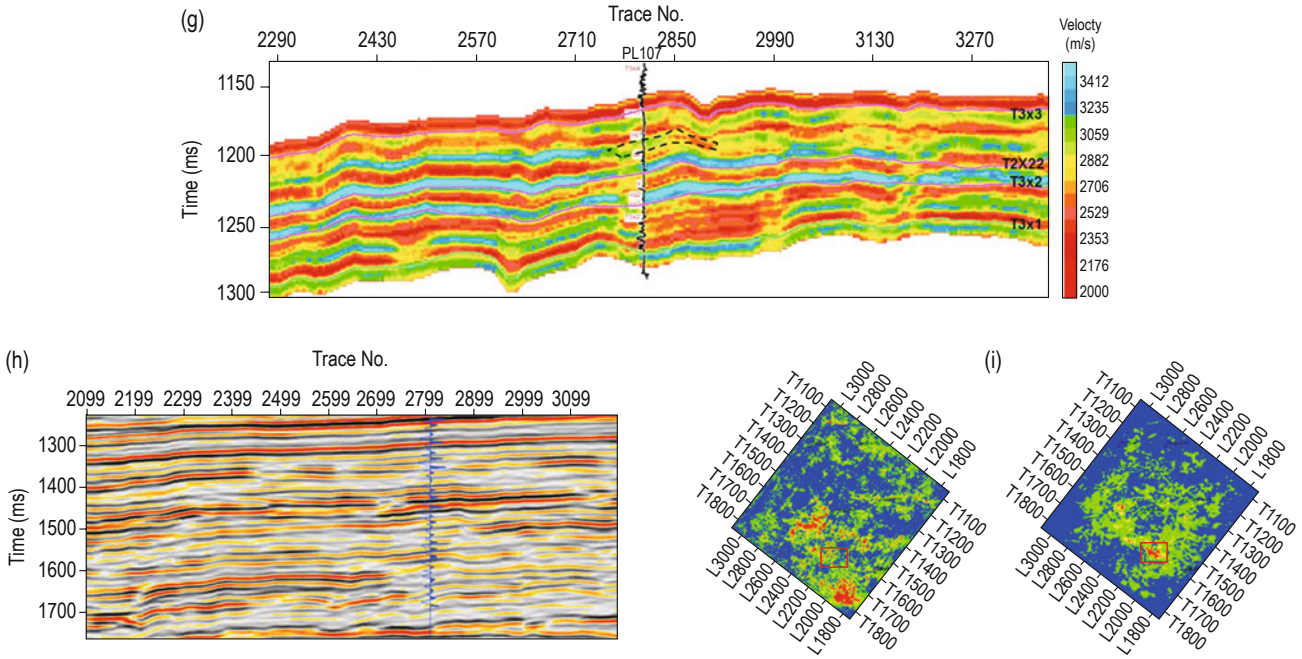

Fig.4 Application results of real converted PS-wave data. (a) Converted PS-wave profile before processing, (b) converted PS-wave profile after high-resolution processing using our proposed method, (c) amplitude spectrum of converted PS-wave before (left) and after (right) high-resolution processing, (d) comparison of converted PS-wave and log data before processing, (e) comparison of converted PS-wave and log data after high-resolution processing, (f) velocity inversion profile of converted PS-wave before high-resolution processing, (g) velocity inversion profile of converted PS-wave after high-resolution processing, (h) high-resolution profile of PP-wave, and (i) attribute analysis results of converted PS-wave (left) and PP-wave (right).

the PP-wave is strong and that of the PS-wave is weak. Based on these results, we can conclude that this method can effectively improve the resolution of converted PS-wave data and that the joint interpretation of the high-resolution converted PS- and PP-waves can also improve the accuracy of oil and gas exploration.

Conclusions

In this paper, we investigated the high-resolution processing of the spectral inversion technique for converted PS-wave data in the Penglai area in the Sichuan Basin. We reached the following conclusions:

1. Based on the basic principle of spectral inversion, we can deduce the objective function of the multi-layer sparse reflection coefficient and improve the accuracy of this reflection coefficient using the least squares inversion algorithm based on the total variation constraint.

2. We can convolute the reflection coefficient obtained by the spectral inversion method and the Gaussian-fitting broadband wavelet to obtain broadband seismic data, which improves the recognition accuracy of thin reservoirs and faults.

3. Results from our theoretical testing and converted PS-wave real data application show that this method can greatly improve the resolution of converted PS-wave data and meet the requirements of multi-wave joint interpretation. It can also provide a clearer fault, richer low-frequency information, and higher resolution data for subsequent multi-wave combined reservoir prediction.

References

Chopra, S., Castagna, J. P., and Portniaguine, O., 2006, Seismic resolution and thin-bed reflectivity inversion: CSEG Recorder, **31**(1), 19−25.

Chopra, S., Castagna, J. P., and Xu. Y., 2009, Thin-bed reflectivity inversion and some applications: First Break **27**(5), 55−62.

Chen, X. H., He, Z. H., Zhu, S. X., et al, 2012, Seismic low-frequency-based calculation of reservoir fluid mobility and its application: Applied Geophysics, **9**(3), 326−332.

Cai, X. L., 2000, Application of Yu wavelet to seismic data

processing: Oil Geophysical Prospecting, **35**(4), 497−507.

Liu, X., Yin, X., Wu, G., et al., 2016, Identification of deep reservoir fluids based on basis pursuit inversion for elastic impedance: Chinese Journal of Geophysics, **59**(1), 277−286

Li, G. F., Xiong, J. L., Zhou, H., et al, 2008, Seismic reflection characteristics of fluvial sand and shale inter-bedded layers: Applied Geophysics, **5**(3), 219−229.

Liu, C., Li, B. N., Zhao, X., et al, 2014, Fluid identification based on frequency-dependent AVO attribute inversion in multi-scale fracture media: Applied Geophysics, **11**(4), 384−394.

Li, G. F., Qin, D. H., Peng, G. X., et al., 2013, Experimental analysis and application of sparsity constrained deconvolution: Applied Geophysics, **10**(2), P191−200.

Long, Y., Han, L. G., Han, L., et al, 2012, Ll norm optimal solution match processing in the wavelet domain: Applied Geophysics, **9**(4), P451−458.

Nguyen, T., and Castagna, J., 2010, High resolution seismic reflectivity inversion: Journal of Seismic Exploration, 303–320.

Oyem, A., and Castagna, J., 2013, Layer thickness estimation from the frequency spectrum of seismic reflection data: 83th Annual International Meeting, SEG, Expanded Abstracts, 1451−1455.

Partyka, G. A., Gridley, J. A., and Lopez, J. A., 1999, Interpretational applications of spectral decomposition in reservoir characterization: The Leading Edge, **18**, 353–360

Portniaguine, O., and Castagna, J. P., 2004, Inverse spectral decomposition: 74th Annual International: Meeting, SEG, Expanded Abstracts, 1786–1789.

Portniaguine, O., Castagna J. P., 2005, Spectral inversion: Lessons from modeling and Boonesville case study: 75th Annual International Meeting, SEG, Expanded Abstracts, 1638−164.

Puryear, C. I., and Castagna, J. P., 2006, An algorithm for calculation of bed thickness and reflection coefficients from amplitude spectrum: 76th Annual International Meeting, SEG, Expanded Abstracts, 1767–1770.

Puryear, C. I., and Castagna, J. P., 2008, Layer-thickness determination and stratigraphic interpretation using spectral inversion: Theory and application: Geophysics, **73**(2), R37–R48.

Yu, S. P., 1996, Wide-band Ricker wavelet: OGP, **V31**(5), 615.

Yuan, S. Y., Wang, S. X., and Tian, N., 2009, Swarm intelligence optimization and its application in geophysical data inversion: Applied Geophysics, **6**(2), 166–174.

Yang, H., Zheng, X. D., Ma, S. F., et al., 2011, Thin-bed reflectivity inversion based on matching pursuit: SEG Technical Program Expanded Abstracts 2011, 2586−2590.

Yuan, S. Y., and Wang, S. X., 2013, Spectral sparse Bayesian learning reflectivity inversion: Geophysical Prospecting, **61**(4), 735–746.

Zhou, D., H., Wang, B., Shen, Z., H., and Peng, G., 2014, Geostatistical spectral inversion: the thin layer study using spectral inversion method with Geostatistical Information: SEG Technical Program Expanded Abstracts, 3272−3276.

Zhang, S. Q., Han, L. G., Li, C., et al., 2015, Computation method for reservoir fluid mobility based on high-resolution inversion spectral decomposition: Geophysical Prospecting for Petroleum, **54**(2), 142−149.

Zhang, L. Y., Wang, Y. C., and Pei, J. Y., 2015, Three-component seismic data in thin interbedded reservoir exploration: Applied Geophysics, **13**(1), 79−85.

Zhang, J. H., Zhang, B. B., Zhang, Z. J., et al., 2015, Low-frequency data analysis and expansion: Applied Geophysics, **12**(2), 212−220.

Zhang, R., and Castagna, J., 2011, Seismic sparse-layer reflectivity inversion using basis pursuit decomposition: Geophysics, **76**(6), R147–R158.

Zhang Hua, Received a master's degree in geophysical and information technology from China University of Petroleum (East China) in 2008, Now study a doctor 's degree in Chengdu University of Technology, And engaged in high resolution processing of seismic data in Geophysical Exploration Company, Chuanqing Drilling Engineering Co. Ltd., CNPC.